Astronomy & Astrophysics manuscript no. Irregulares
March 18, 2015

Astrometric positions for 18 irregular satellites of giant planets from 23 years of observations[⋆,⋆⋆,⋆⋆⋆]

A. R. Gomes-Júnior[1], M. Assafin[1,⋆⋆⋆⋆], R. Vieira-Martins[1,2,3,†], J.-E. Arlot[4], J. I. B. Camargo[2,3], F. Braga-Ribas[2,4], D. N. da Silva Neto[5], A. H. Andrei[1,2,‡], A. Dias-Oliveira[2], B. E. Morgado[1], G. Benedetti-Rossi[2]

[1] Observatório do Valongo/UFRJ, Ladeira Pedro Antônio 43, CEP 20.080-090 Rio de Janeiro - RJ, Brazil
e-mail: altair08@astro.ufrj.br
[2] Observatório Nacional/MCT, R. General José Cristino 77, CEP 20921-400 Rio de Janeiro - RJ, Brazil
e-mail: rvm@on.br
[3] Laboratório Interinstitucional de e-Astronomia - LIneA, Rua Gal. José Cristino 77, Rio de Janeiro, RJ 20921-400, Brazil
[4] Institut de mécanique céleste et de calcul des éphémérides - Observatoire de Pares, UMR 8028 du CNRS, 77 Av. Denfert-Rochereau, 75014 Paris, France
e-mail: arlot@imcce.fr
[5] Centro Universitário Estadual da Zona Oeste, Av. Manual Caldeira de Alvarenga 1203, CEP 23.070-200 Rio de Janeiro RJ, Brazil

Received ; accepted

ABSTRACT

Context. The irregular satellites of the giant planets are believed to have been captured during the evolution of the solar system. Knowing their physical parameters, such as size, density and albedo is important to constrain where they came from and how they were captured. The best way to obtain these parameters are observations in loco by spacecrafts or from stellar occultations by the objects. Both techniques demand that the orbits are well known.
Aims. We aimed to obtain good astrometric positions of irregular satellites in order to improve their orbits and ephemeris.
Methods. We identified and reduced observations of several irregular satellites from three database containing more than eight thousand images obtained between 1992 and 2014 at three sites (Observatório do Pico dos Dias, Observatoire de Haute-Provence and European Southern Observatory - La Silla). We used the software PRAIA (Platform for Reduction of Astronomical Images Automatically) to make the astrometric reduction of the CCD frames. The UCAC4 catalogue represented the International Celestial Reference System in the reductions. The identification of the satellites in the frames was done through their ephemerides as determined from the SPICE/NAIF kernels. Some procedures were taken to overcome missing or incomplete information (coordinates, date), mostly for the older images.
Results. We managed to obtain more than 6000 positions for 18 irregular satellites, being 12 of Jupiter, 4 of Saturn, 1 of Uranus (Sycorax) and 1 of Neptune (Nereid). For some satellites the number of obtained positions is more than 50% of that used in earlier orbital numerical integrations.
Conclusions. Comparison of our positions with recent JPL ephemeris suggests the presence of systematic errors in the orbits of at least a few irregular satellites. The most evident case was an error in the inclination of Carme.

Key words. Planets and satellites: general - Astrometry: individual: Jovian and Saturnian irregular satellites

1. Introduction

The irregular satellites of the giant planets are smaller than the regular moons, having more eccentric, inclined, distant and, in most cases, retrograde orbits. Due to their orbital configurations, it is largely accepted that these objects were captured in the early solar system (Sheppard & Jewitt 2003).

Because they are faint, the majority of these objects was discovery only in the last decade[1] . They were never visited by a spacecraft, with the exception of Himalia and Phoebe, in a flyby by the Cassini space probe in 2000 for Himalia (Porco et al. 2003) and in 2004 for Phoebe (Desmars et al. 2013).

Send offprint requests to: A. R. Gomes-Júnior
⋆ The complete version of Table 8 is only available through CDS.
⋆⋆ Based on observations made at Laboratório Nacional de Astrofísica (LNA), Itajubá-MG, Brazil.
⋆⋆⋆ Partially based on observations through the ESO runs 079.A-9202(A), 075.C-0154, 077.C-0283 and 079.C-0345.
⋆⋆⋆⋆ Associate researcher at Observatoire de Paris/IMCCE, 77 Avenue Denfert Rochereau 75014 Paris, France
† Associate researcher at Observatoire de Paris/IMCCE, 77 Avenue Denfert Rochereau 75014 Paris, France
‡ Associated researcher at the Observatoire de Paris/SYRTE, 77 av. Denfert Rochereau, 75014 Paris, France

[1] Website: http://ssd.jpl.nasa.gov/?sat_discovery

There is a number of capture mechanisms of objects by giant planets proposed in the literature. There is the Gas Drag in the primordial circumplanetary nebulae (Sheppard 2006) where the object would be affected by the gas drag and its velocity slowed down until it be captured by the planet. Another mechanism is called pull-down capture (Sheppard 2006), where the mass of the planet would increase while the object was temporarily captured.

A mechanism based in the Nice model (Morbidelli et al. 2005; Tsiganis et al. 2005; Gomes et al. 2005) was proposed by Nesvorný et al. 2007 and, in the specific case of Jupiter with the modern Nice model, by Nesvorný et al. 2014. During the early solar system instability, encounters between the outer planets occurred. These planetary encounters could exchange energy and angular momentum between planets and the objects nearby making it possible for the capture of irregular bodies by the giant planets. In this scenario, the survival rate of prior-LHB (Late Heavy Bombardment) satellites is very small.

Another important mechanism is the capture through collisional interactions (Sheppard 2006). A collision between two small bodies in the Hill's sphere of the planet could generate fragmented objects and the dissipated energy could be such that some of these objects could be captured.

Some of these objects are in dynamical groups with similar orbital elements, called families, similar to families found in the Main Asteroid Belt. These families may have been created by a parent body disrupted by collisions with comets or other satellites (Nesvorný et al. 2004). Collisions with comets are more likely to have occurred during the Late Heavy Bombardment (LHB) (Gomes et al. 2005).

Nesvorný et al. 2003 studied the collision rates between irregular satellites and concluded that some satellites could have been removed by collision with a bigger satellite. The rate collision between satellites of the Himalia Group (Himalia, Elara, Lysithea and Leda, mainly), for instance, was found to be more than 1 during the solar system age suggesting that their current structure was originated by satellite-satellite collision.

For Phoebe, ejected material from its surface caused by impacts could evolve due to Poynting-Robertson drag and collide with Iapetus causing the large variation in albedo observed on it (Nesvorný et al. 2003). Indeed, Cassini was able to detected in Phoebe an absorption feature at 2.42 μm (probably CN combinations) that was also detected in the dark side of Iapetus (Clark et al. 2005).

If these objects were captured, there remains the question of where they came from. Clark et al. 2005 showed from imaging spectroscopy from Cassini that Phoebe has a surface probably covered by material from the outer solar system and Grav et al. 2003 showed that the satellites of the Jovian Prograde Group Himalia have grey colors implying that their surfaces are similar to that of C-type asteroids. In that same work, the Jovian Retrograde Group Carme was found to have surface colors similar to the D-type asteroids like Hilda or Trojan families while JXIII Kalyke has a redder color like Centaurs or trans-neptunian objects (TNOs).

For Saturnian satellites, Grav & Bauer 2007 showed by their colors and spectral slopes that these satellites contain a more or less equal fraction of C-, P- and D-like objects but SXXII Ijiraq is marginally redder than D-type objects. These works may suggest different origins for the irregular satellites.

In this context, we used 3 databases for deriving precise positions for the irregular satellites observed at Observatório do Pico dos Dias (1.6 m and 0.6 m telescopes, IAU code 874), Observatoire Haute-Provence (1.2m telescope, IAU code 511) and ESO (2.2 m telescope, IAU code 809). Many irregular satellites were observed between 1992 and 2014 covering a few orbital periods of these objects (12 satellites of Jupiter, 4 of Saturn, Sycorax of Uranus and Nereid of Neptune). The positions derived from the observations can be used in orbital new numerical integrations, generating more precise ephemerides. Stellar occultations by these satellites could then be better predicted. Once observed, they will make it possible to obtain the satellites' physical parameters (shape, size, albedo, density) with unprecedented precision. The knowledge of these parameters would in turn bring valuable information for the study of the capture mechanisms and origin of the irregular satellites.

The databases are described in Sect. 2. The astrometric procedures in Sect. 3. The obtained positions are presented in Sect 4 and analysed in Sect. 5. Conclusions are given in Sect. 6.

2. Databases

Our three databases consist in optical CCD images from many observational programs performed with different telescopes/detectors targeting a variety of objects, among which irregular satellites. The observations were made at 3 sites: Observatório do Pico dos Dias (OPD), Observatoire Haute-Provence (OHP) and European Southern Observatory (ESO). Altogether there are more than 8 thousand FITS images obtained in a large time span (1992-2014) for the irregular satellites. Since the OHP and mostly the OPD database registers were not well organized, we had to start from scratch and develop an automatic procedure to identify and filter only the images of interest, that is, of the irregular satellites. The instruments and images characteristics are described in the following subsections.

2.1. OPD

The OPD database was produced at Observatório do Pico dos Dias (OPD, IAU code 874)[2], located at geographical longitude $+45^\circ\ 34'\ 57''$, latitude $-22^\circ\ 32'\ 04''$ and an altitude of 1864 m, in Brazil. The observations were made between 1992 and 2014 by our group in a variety of observational programs. In Fig 1 we plot the number of frames obtained per satellite over time and in Fig 2 the number of frames per satellite for each telescope. Two telescopes of 0.6 m diameter (Zeiss and Boller & Chivens) and one 1.6 m diameter (Perkin-Elmer) were used for the observations. It was identified 5248 observations containing irregular satellites, being 3168 from the Boller & Chivens, 1967 from the Perkin-Elmer and 113 from the Zeiss.

This is an inhomogeneous database with observations made with 9 different detectors (see Table 1) and 6 different filters. The headers of most of the older FITS images had missing, incomplete or incorrect coordinates or date. In some cases, we could not identify the detector origin. The procedures used to overcome these problems are described in Sect. 3.

[2] Website: http://www.lna.br/opd/opd.html - in Portuguese

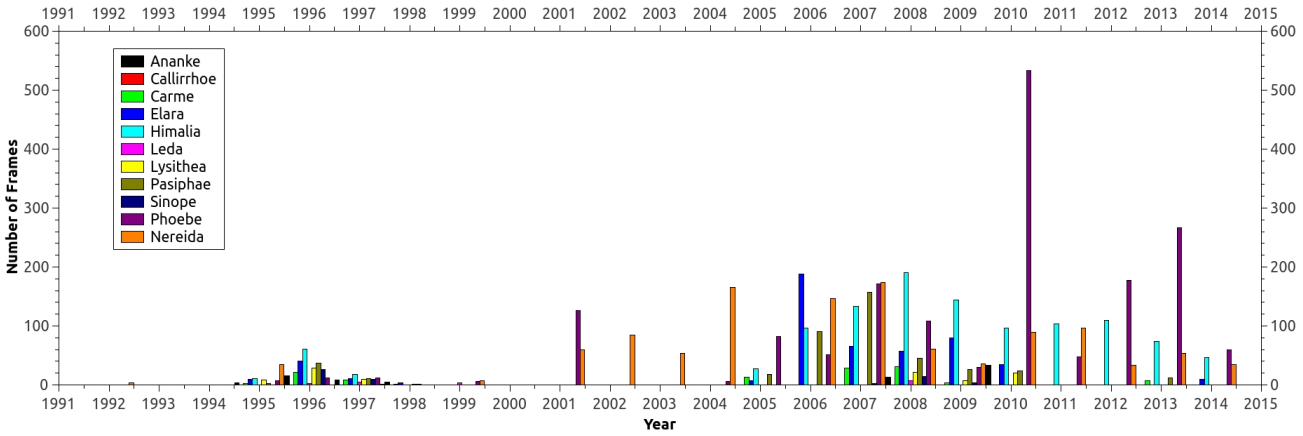

Fig. 1. Distribution of observations of the satellites over time at OPD.

Table 1. Characteristics of OPD detectors used in this work.

Perkin-Elmer		
Detector	Field of View (arcmin)	Pixel Scale ("/px)
CCD048	770 x 1152	22.5
CCD098	2048 x 2048	13.5
CCD101	1024 x 1024	24.0
CCD105	2048 x 2048	13.5
CCD106	1024 x 1024	24.0
CCD301	385 x 578	22.0
CCD523	455 x 512	19.0
IKON	2048 x 2048	13.5
IXON	1024 x 1024	13.5

The plate scale of the telescopes are 13.09"/mm for Perkin-Elmer, 25.09"/mm for Boller & Chivens and 27.5"/mm for Zeiss.

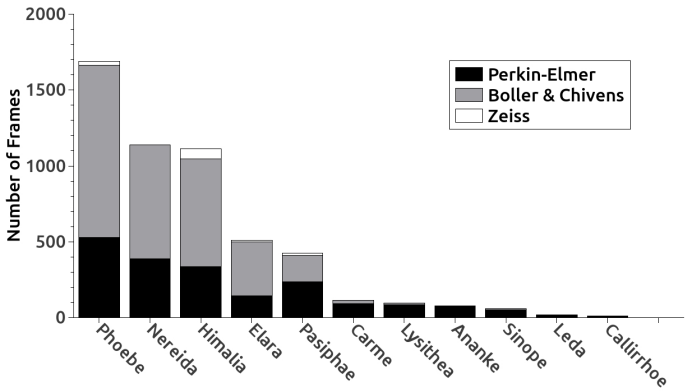

Fig. 2. Number of frames observed per satellite by OPD telescope.

2.2. OHP

The instrument used at the Observatoire de Haute Provence (OHP, IAU code 511, 5° 42′ 56.5″ E, 43° 55′ 54.7″N, 633.9 m) was the 1.2m-telescope in a Newton configuration. The focal length is 7.2 m. The observations were made between 1997 and 2008. During this time only one CCD detector 1024×1024 was used. The size of field is 12′×12′ with a pixel scale of 0.69″. All the images were acquired without the use of filters. Fig. 3 shows the distribution of the observation of the satellites over time and Fig. 4 the number of frames

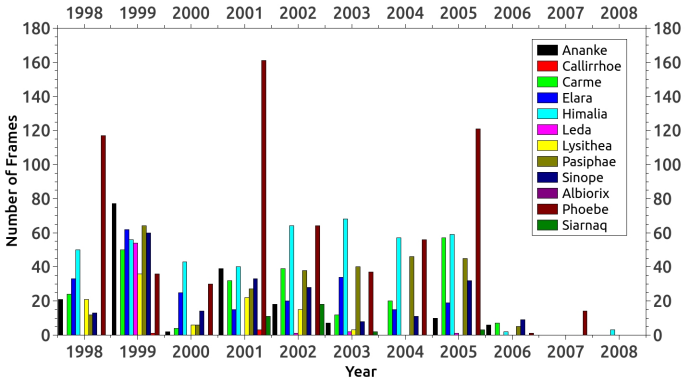

Fig. 3. Distribution of the observations of the satellites over time from observations at OHP.

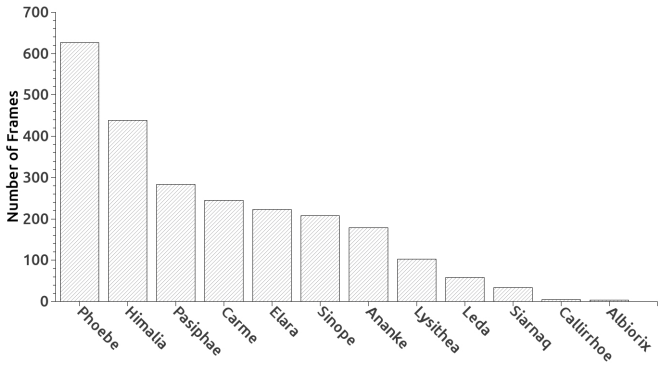

Fig. 4. Number of frames per satellite observed at OHP.

observed for each satellite. From these observations, 2408 were identified containing irregular satellites.

2.3. ESO

Observations were made at the 2.2 m Max-Planck ESbyO (ESO2p2) telescope (IAU code 809) with the Wide Field Imager (WFI) CCD mosaic detector. Each mosaic is composed by eight CCDs of 7.5′ × 15′ (α, δ) sizes, resulting in a total coverage of 30′×30′ per mosaic. Each CCD has $4k \times 2k$ pixels with a pixel scale of 0.238″. The filter used was a broad-band R filter (ESO#844) with $\lambda_c = 651.725$ nm and $\Delta\lambda = 162.184$ nm. The telescope was shifted between ex-

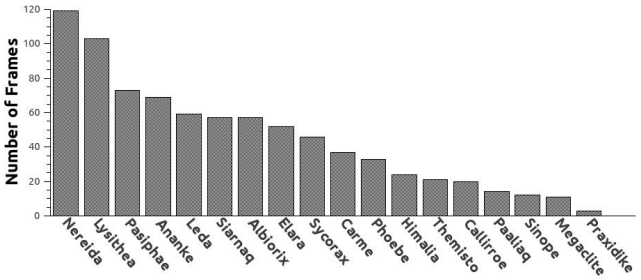

Fig. 5. Number of frames per satellite observed at ESO.

posures in such a way that each satellite was observed at least twice in different CCDs.

The satellites were observed in 24 nights, divided in 5 runs, between April 2007 and May 2009 in paralel with, and using the same observational and astrometric procedures of the program that observed stars along the sky path of transneptunian objects (TNOs) to identify candidates to stellar occultation (see Assafin et al. (2010, 2012); Camargo et al. (2014)). A total of 810 observations for irregular satellites were obtained. Fig 5 shows the number of frames per satellite.

3. Astrometry

Almost all the frames were photometrically calibrated with auxiliary bias and flat-field frames by means of standard procedures using IRAF[3] and, for the mosaics, using the esowfi (Jones & Valdes 2000) and mscred (Valdes 1998) packages. Some of the nights at OPD didn't have bias and flat-field images so the correction was not possible.

The astrometric treatment was made with the Platform for Reduction of Astronomical Images Automatically (PRAIA) (Assafin et al. 2011). The (x, y) measurements were performed with 2-dimensional circular symmetric Gaussian fits within 1 Full Width Half Maximum (FWHM = seeing). Within 1 FWHM, the image profile is well described by a Gaussian profile, free from the wing distortions, which may jeopardize the center determination. PRAIA automatically recognizes catalog stars and determines (α, δ) with a user-defined model relating the (x, y) measured and (X, Y) standard coordinates projected in the sky tangent plane.

We used the UCAC4 (Zacharias et al. 2013) as the practical representative of the International Celestial Reference System (ICRS). For each frame, we used the six constants polynomial model to relate the (x, y) measurements with the (X, Y) tangent plane coordinates. For ESO, we followed the same astrometric procedures described in detail in Assafin et al. (2012); the (x, y) measurements of the individual CCDs were pre-corrected by a field distortion pattern, and all positions coming from different CCDs and mosaics were then combined using a 3rd degree polynomial model to produce a global solution for each night and field observed, and final (α, δ) object positions were obtained in the UCAC4 system.

In Table 2 we list the average mean error in α and δ for the reference stars obtained by telescope, the average (x, y) measurement errors of the Gaussian fits described above and the mean number of UCAC4 stars used by frame.

Table 2. Astrometric (α, δ) reduction by telescope.

Telescope	Mean errors σ_α mas	σ_δ mas	UCAC4 stars	Gaus. errors x mas	y mas
PE(OPD)	51	48	24	15	15
B&C (OPD)	56	55	36	29	29
Zeiss (OPD)	58	57	95	26	26
OHP	50	49	46	26	26
ESO	26	25	632	15	15

Mean errors are the standard deviations in the (O−C) residuals from (α, δ) reductions with the UCAC4 catalog. Gaussian errors are the errors in the Gaussian fit used to perform the (x, y) measurements.

For all databases, about 20% of outlier reference stars were eliminated for presenting (O-C) position residuals higher than 120 mas in the (α, δ) reductions.

To help identifying the satellites in the frames, and derive the ephemeris for the instants of the observations for comparisons (see Sect 5), we used the kernels from SPICE/JPL[4]. The JPL ephemeris that represented the Jovian satellites was the DE421 + JUP300. For the Saturnian satellites the ephemeris was DE421 + SAT359 to Hyperion, Iapetus and Phoebe and DE421 + SAT361 to Albiorix, Siarnaq and Paaliaq. The DE421 + URA095 was used for Sycorax and DE421 + NEP081 for Nereid. More recent ephemeris versions became available after completion of this work, but this did not affect the results.

In the OPD database, there were some images (mostly the older ones) with missing coordinates or wrong date in their headers. In the case of missing or wrong coordinates, we adopted the ephemeris as the central coordinates of the frames. When the time was not correct, the FOV identification failed. In this case, a search for wrong date (year) displaying was performed. Problems like registering local time instead of UTC were also identified and corrected.

In all databases, for each night a sigma-clipping procedure was performed to eliminate discrepant positions (outliers). A threshold of 120 mas and a deviation of more than 2.5 sigmas from the nightly average ephemeris offsets were adopted.

From Table 3 to 7 we list the average dispersion (standard deviation) of the position offsets with regard to the ephemeris for α and δ obtained by telescope for each satellite. The final number of frames, number of nights (in parenthesis), the mean number of UCAC4 stars used in the reduction and the approximate V magnitude are also given. The dashed lines separate the satellites from different families with similar orbital parameters: Himalia Group (Himalia, Elara, Lysithea and Leda), Pasiphae Group (Pasiphae, Callirrhoe and Megaclite) and Ananke Group (Ananke and Praxidike). Carme and Sinope are the only samples of their groups. From Saturn, Siarnaq and Paaliaq are from the Inuit Group while Phoebe and Albiorix are the only samples of their groups.

The differences in the dispersion of the ephemeris offsets of the same satellite for distinct telescopes seen in Tables 3 to 7 are caused by the different distribution of observations along the orbit for each telescope. This can be seen in Fig 6 for Carme, 7 for Pasiphae and for all objects in the online

[3] Website: http://iraf.noao.edu/

[4] Website: http://naif.jpl.nasa.gov/naif/toolkit.html

Table 3. Astrometric (α, δ) reduction for each satellite observed with the Perkin-Elmer telescope.

Perkin-Elmer					
Satellite	Offsets (sigma) σ_α mas	σ_δ mas	Nr frames (nights)	UCAC4 stars	Mag
Himalia	290	45	238 (18)	37	14
Elara	230	118	99 (12)	32	16
Lysithea	107	79	53 (8)	41	18
Leda	207	79	6 (2)	46	19
Pasiphae	157	92	144 (13)	22	17
Callirrhoe	66	35	9 (1)	3	21
Carme	97	94	68 (7)	49	18
Sinope	155	77	37 (8)	42	18
Ananke	93	185	52 (7)	40	19
Phoebe	73	95	410 (22)	6	16
Nereid	200	142	289 (29)	8	19

The offsets (sigma) are the average standard deviations of the ephemeris offsets from the (α, δ) positions of the satellites. Also given are the approximate satellite V magnitude and the average number of UCAC4 reference stars per frame.

Table 4. Astrometric (α, δ) reduction for each satellite observed with the Boller & Chivens telescope.

Boller & Chivens					
Satellite	Offsets (sigma) σ_α mas	σ_δ mas	Nr frames (nights)	UCAC4 stars	Mag
Himalia	83	43	560 (31)	57	14
Elara	55	43	294 (23)	53	16
Lysithea	23	42	7 (2)	60	18
Pasiphae	128	71	140 (14)	57	17
Carme	68	111	22 (4)	45	18
Sinope	59	17	4 (1)	22	18
Phoebe	43	48	810 (42)	17	16
Nereid	61	45	514 (38)	20	19

Same as in Table 3.

Table 5. Astrometric (α, δ) reduction for each satellite observed with the Zeiss telescope.

Zeiss					
Satellite	Offsets (sigma) σ_α mas	σ_δ mas	Nr frames (nights)	UCAC4 stars	Mag
Himalia	112	72	56 (4)	91	14
Elara	17	21	10 (1)	146	16
Pasiphae	24	25	11 (1)	140	17
Phoebe	37	30	19 (1)	16	16

Same as in Table 3.

material. Since the observations cover different segments of the orbit, the dispersion of the offsets may vary for different telescopes for a single satellite, with larger covered segments usually implying in larger dispersions and vice-versa. For Nereid, due to its high eccentric orbit, the observations are located between 90° and 270° of True Anomaly where Nereid remains most of the time.

No solar phase correction was applied to the positions. For the biggest irregular satellite of Jupiter, Himalia, it was verified that the maximum deviation in the position due to phase angle is 1.94 *mas* using the phase correction described in Lindegren (1977). For the other satellites, which are smaller objects, this deviation is even smaller. Since our position error is one order of magnitude higher, this effect was neglected.

Table 6. Astrometric (α, δ) reduction for each satellite observed with the OHP telescope.

OHP					
Satellite	Offsets (sigma) σ_α mas	σ_δ mas	Nr frames (nights)	UCAC4 stars	Mag
Himalia	49	66	357 (43)	49	14
Elara	52	61	187 (25)	37	16
Lysithea	63	50	84 (13)	56	18
Leda	118	33	48 (7)	14	19
Pasiphae	101	75	248 (32)	39	17
Carme	114	96	204 (29)	39	18
Sinope	196	73	169 (25)	43	18
Ananke	100	89	141 (20)	62	19
Phoebe	30	31	516 (63)	51	16
Siarnaq	46	98	20 (6)	32	20

Same as in Table 3.

Table 7. Astrometric (α, δ) reduction for each satellite observed with the ESO telescope.

ESO					
Satellite	Offsets (sigma) σ_α mas	σ_δ mas	Nr frames (nights)	UCAC4 stars	Mag
Himalia	76	74	23 (2)	1153	14
Elara	112	87	46 (4)	1492	16
Lysithea	76	88	90 (6)	695	18
Leda	60	125	44 (3)	632	19
Pasiphae	70	114	66 (5)	836	17
Callirrhoe	29	33	16 (1)	493	21
Megaclite	52	34	10 (1)	445	22
Ananke	225	19	57 (3)	761	18
Praxidike	7	38	2 (1)	1934	21
Carme	140	110	37 (4)	1074	18
Sinope	339	70	11 (2)	1542	18
Themisto	894	28	16 (2)	1232	21
Phoebe	102	57	32 (5)	312	16
Siarnaq	86	66	56 (6)	283	20
Paaliaq	301	59	11 (4)	382	21
Albiorix	76	50	46 (6)	330	20
Sycorax	150	82	35 (9)	375	21
Nereid	115	78	99 (12)	362	19

Same as in Table 3.

4. Satellite positions

The final set of positions of the satellites consists in 6523 catalogued positions observed between 1992 and 2014 for 12 satellites of Jupiter, 4 of Saturn, 1 of Uranus and 1 of Neptune. The topocentric positions are in the ICRS. The catalogues (one for each satellite) contain epoch of observations, the position error, filter used, estimated magnitude (from PSF fitting) and telescope origin. The magnitude errors can be as high as 1 mag; they are not photometrically calibrated and should be used with care. The position errors

Table 9. Comparison of positions obtained with Jacobson et al. 2012.

	Number of Positions				
Satellite	OPD	OHP	ESO	Total	Jacobson
Himalia	854	357	23	1234	1757
Elara	403	187	46	636	1115
Lysithea	60	84	90	234	431
Leda	6	48	44	98	178
Pasiphae	295	248	66	609	1629
Callirrhoe	9	-	16	25	95
Megaclite	-	-	10	10	50
Ananke	52	141	57	250	600
Praxidike	-	-	2	2	59
Carme	90	204	37	331	973
Sinope	41	169	11	221	854
Themisto	-	-	16	16	55
Phoebe	1239	516	32	1787	3479
Siarnaq	-	20	56	76	239
Paaliaq	-	-	11	11	82
Albiorix	-	-	46	50	137
Sycorax	-	-	35	35	237
Nereid	803	-	99	902	716

Comparison between the number of positions obtained in our work with the number used in the numerical integration of orbits by the JPL as published by Jacobson et al. 2012.

were estimated from the dispersion of the ephemeris offsets of the night of observation of each position. Thus, these position errors are probably overestimated, as there must be ephemeris errors present in the dispersion of the offsets. These position catalogues are freely available in electronic form at the CDS (see a sample in Table 8).

The number of positions acquired is significant compared to the number used in the numerical integration of orbits by the JPL (Jacobson et al. 2012) as shown in Table 9.

5. Comparison with ephemeris

Intending to see the potential of our results to improve the orbit of the irregular satellites observed, we analysed the offsets of our positions with regard to the ephemeris mentioned in Sect. 3. Taking Carme as example, we plot in Fig. 6 the mean ephemeris offsets for each night and their dispersions (1 sigma error bars) as a function of the true anomaly in right ascension (6a) and declination (6b). Fig. 6b clearly shows a systematic error in declination. When Carme is close to its apojove (true anomaly = 180°) its offsets are more likely to be more negative than those close to its perijove (true anomaly = 0°). The offsets obtained from observations by 4 telescopes using different cameras and filters are in good agreement, meaning that there is an error in the ephemeris of Carme, most probably due to an error in its orbital inclination.

This pattern in declination was also seen for other satellites like Pasiphae (Fig: 7) and Ananke (plots for other satellites with significant number of observations can be seen in the online material. For some satellites, the orbital coverage is not enough to clearly indicate the presence of systematic errors in specific orbital elements. However, comparing the internal position mean errors of the reductions (Table 2) with the external position errors estimated from the dispersion of the ephemeris offsets (Tables 3 to 7), we see position error values much larger than expected from the mean errors. This means that besides some expected astrometric errors, significant ephemeris errors must also be present.

6. Conclusions

The positions of all the objects were determined using the PRAIA package. The package was suited to cope with the huge amount of observations and the task of identifying the satellites within the database. PRAIA tasks were also useful to deal with the missing or incorrect coordinate and time stamps present mostly in the old observations. The UCAC4 was used as the reference frame.

We managed a large database with more than 100 thousand FITS images acquired by 5 telescopes in 3 sites between 1992 and 2014. From that, we identified 8466 observations of irregular satellites, from which we managed to obtain 6523 suitable astrometric positions, giving a total of 3666 positions for 12 satellites of Jupiter, 1920 positions for 4 satellites of Saturn, 35 positions for Sycorax (Uranus) and 902 positions for Nereid (Neptune).

For some satellites the number is comparable to the number used in the numerical integration of orbits by the JPL (Jacobson et al. 2012) (see Table 9). Systematic errors in the ephemeris were found for at least some satellites (Ananke, Carme, Elara and Pasiphae). In the case of Carme, we evidenced an error in the orbital inclination.

Acknowledgements. The author thanks the financial support of CAPES. M. A. thanks the CNPq (Grants 473002/2013-2 and 308721/2011-0) and FAPERJ (Grant E-26/111.488/2013). RVM aknowledges CNPq grant 306885/2013-1 and CAPES/COFECUB grant 791/13.

References

Assafin, M., Camargo, J. I. B., Vieira Martins, R., et al. 2010, Astronomy and Astrophysics, 515, A32
Assafin, M., Camargo, J. I. B., Vieira Martins, R., et al. 2012, Astronomy and Astrophysics, 541, A142
Assafin, M., Vieira Martins, R., Camargo, J. I. B., et al. 2011, in Gaia follow-up network for the solar system objects : Gaia FUN-SSO workshop proceedings, held at IMCCE -Paris Observatory, France, November 29 - December 1, 2010. ISBN 2-910015-63-7, ed. P. Tanga & W. Thuillot, 85–88
Camargo, J. et al. 2014, Astronomy and Astrophysics, 561, 10 pgs
Clark, R. N. et al. 2005, Nature, 435, 66
Desmars, J. et al. 2013, Astronomy and Astrophysics, 553
Gomes, R., Levison, H. F., Tsiganis, K., & Morbidelli, A. 2005, Nature, 435, 466
Grav, T. & Bauer, J. 2007, Icarus, 191, 267
Grav, T., Holman, M. J., Gladman, B. J., & Aksnes, K. 2003, Icarus, 166, 33
Jacobson, R. et al. 2012, The Astronomical Journal, 144, 8 pgs
Jones, H. & Valdes, F. 2000, in "Handling ESO WFI Data With IRAF", ESO Document number 2p2-MAN-ESO-22200-00002
Lindegren, L. 1977, Astronomy and Astrophysics, 57, 55
Morbidelli, A., Levison, H. F., Tsiganis, K., & Gomes, R. 2005, Nature, 435, 462
Nesvorný, D., Alvarellos, J. L. A., Dones, L., & Harold, L. 2003, The Astronomical Journal, 126, 398
Nesvorný, D., Beaugé, C., & Dones, L. 2004, The Astronomical Journal, 127, 1768
Nesvorný, D., Vokrouhlický, D., & Deienno, R. 2014, The Astronomical Journal, 784, 22
Nesvorný, D., Vokrouhlický, D., & Morbidelly, A. 2007, The Astronomical Journal, 133, 1962
Porco, C. et al. 2003, Science, 299, 1541

Table 8. CDS data table sample.

Himalia								
RA (ICRS)		Dec	RA error	Dec error	Epoch	Mag	Filter	Telescope
h m	s	° ′ ″	(mas)	(mas)	(jd)			
16 59	11.6508	-22 00 44.855	17	12	2454147.78241319	16.0	C	BC
16 59	11.6845	-22 00 44.932	17	12	2454147.78332384	15.8	C	BC
16 59	11.7181	-22 00 44.978	17	12	2454147.78422477	16.0	C	BC
16 59	11.7818	-22 00 45.143	17	12	2454147.78602662	15.9	C	BC
16 59	11.8188	-22 00 45.232	17	12	2454147.78693750	16.0	C	BC
17 17	11.0344	-22 47 19.415	30	24	2454205.63885463	16.1	U	BC
17 17	11.0270	-22 47 19.381	30	24	2454205.63959167	16.1	U	BC
17 17	11.0258	-22 47 19.366	30	24	2454205.64031875	16.1	U	BC
17 17	11.0192	-22 47 19.417	30	24	2454205.64104583	16.1	U	BC

This sample corresponds to 9 observations of Himalia from February 16, 2007 and April 15, 2007. Tables contain the topocentric ICRS coordinates of the irregular satellites, the position error estimated from the dispersion of the ephemeris offsets of the night of observation, the estimated magnitude, the filter used and telescope origin. The filters may be U, B, V, R or I following the Johnson system; C stands for clear (no filter used), resulting in a broader R band magnitude, RE for the broad-band R filter ESO#844 with $\lambda_c = 651.725$ nm and $\Delta\lambda = 162.184$ nm (full width at half maximum) and "un" for unknown filter. E, OH, PE, BC and Z stand respectively for the ESO, OHP, Perkin-Elmer, Bollen & Chivens and Zeiss telescopes.

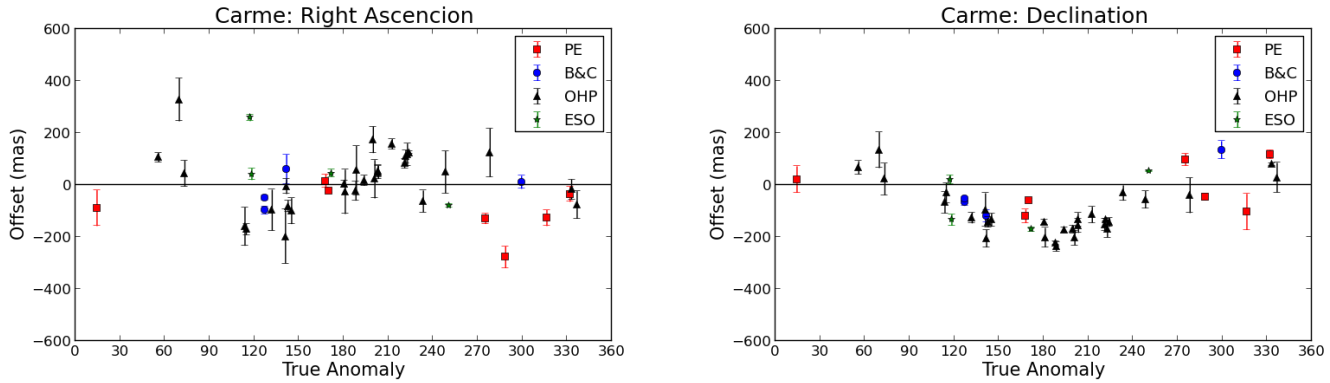

(a) Right Ascension (b) Declination

Fig. 6. Mean ephemeris offsets and dispersions (1 sigma error bars) in the coordinates of Carme taken night by night by true anomaly for each telescope.

Sheppard, S. S. 2006, in "Outer Irregular Satellites of the Planets and Their Relationship with Asteroids, Comets and Kuiper Belt Objects", IAU Symposium No. 229, 2006, pgs 319-334
Sheppard, S. S. & Jewitt, D. C. 2003, Nature, 423, 261
Tsiganis, K., Gomes, R., Morbidelli, A., & Levison, H. F. 2005, Nature, 435, 459
Valdes, F. G. 1998, in "The IRAF Mosaic Data Reduction Package" in Astronomical Data Analysis Software and Systems VII, A.S.P. Conference Ser., Vol 145, eds R. Albrecht, R. N. Hook and H. A. Bushouse, 53
Zacharias, N., Finch, C. T., Girard, T. M., et al. 2013, AJ, 145, 44

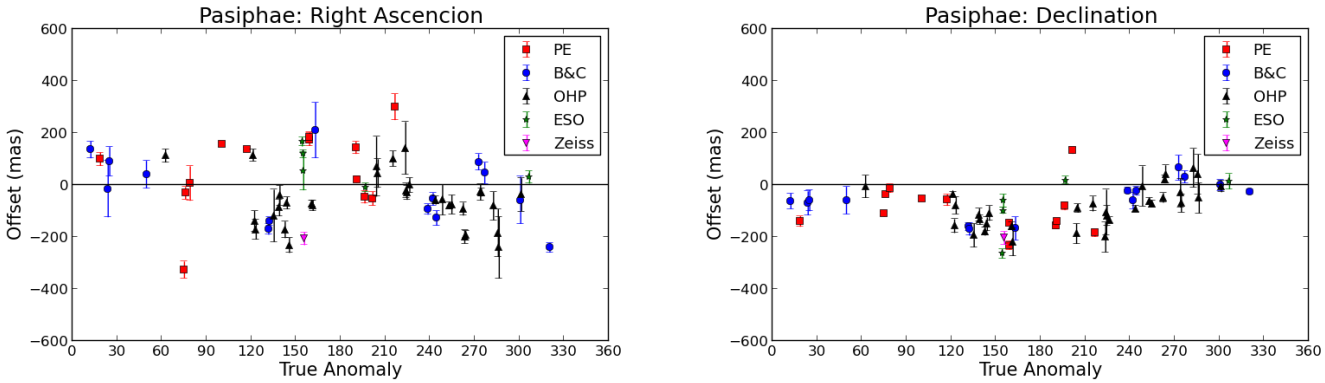

(a) Right Ascension (b) Declination

Fig. 7. Same as in Fig 6 for Pasiphae.

Appendix A: Ephemeris offsets as a function of true anomaly for all observed irregular satellites

The distribution of ephemeris offsets along the orbit of the satellites are shown below. The red square is for the observations with the Perkin-Elmer telescope from OPD, the blue circle for Boller & Chivens, the magenta triangle down for Zeiss, the black triangle up for OHP and the green star for ESO.

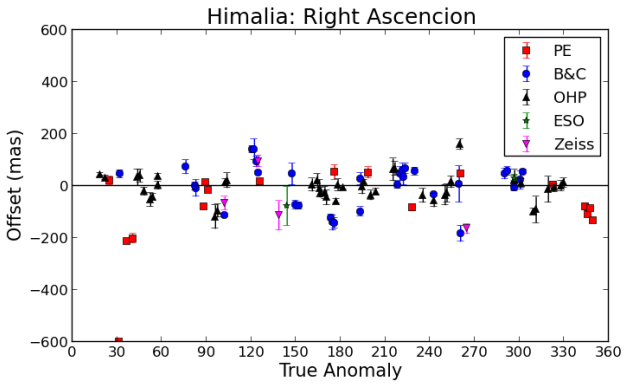

(a) Right Ascension

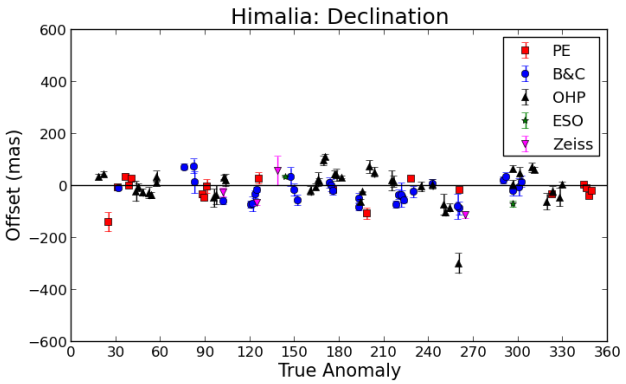

(b) Declination

Fig. A.1. Mean ephemeris offset and dispersion (1 sigma error bars) in the coordinates of Himalia taken night by night as a function of true anomaly.

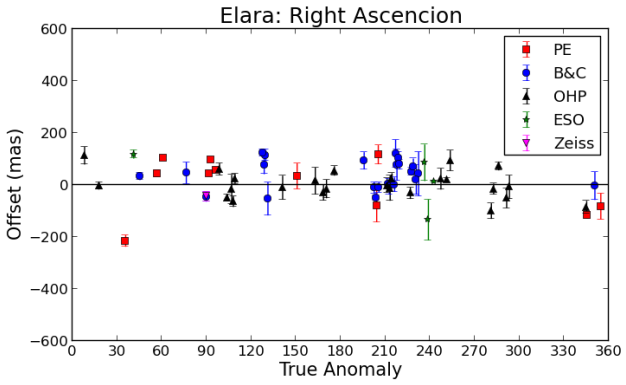

(a) Right Ascension

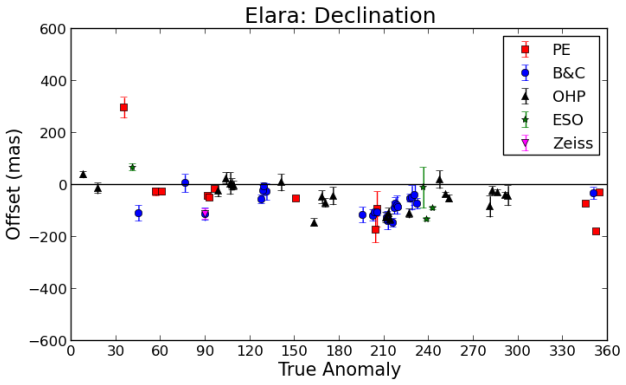

(b) Declination

Fig. A.2. Same as in Fig A.1 for Elara.

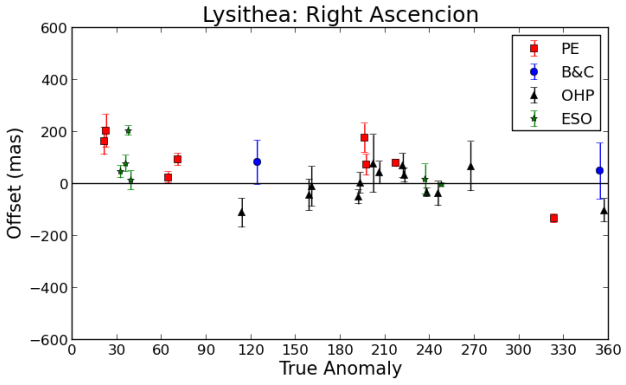

(a) Right Ascension

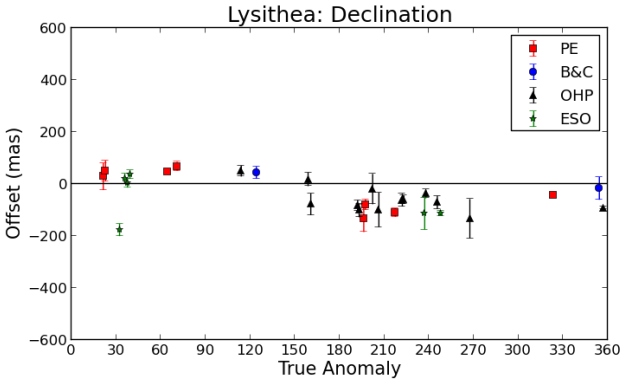

(b) Declination

Fig. A.3. Same as in Fig A.1 for Lysithea.

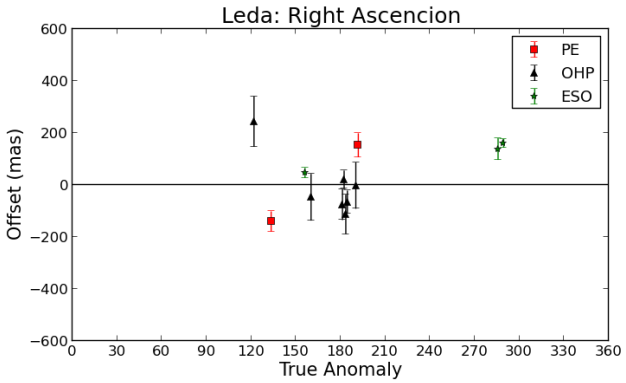

(a) Right Ascension

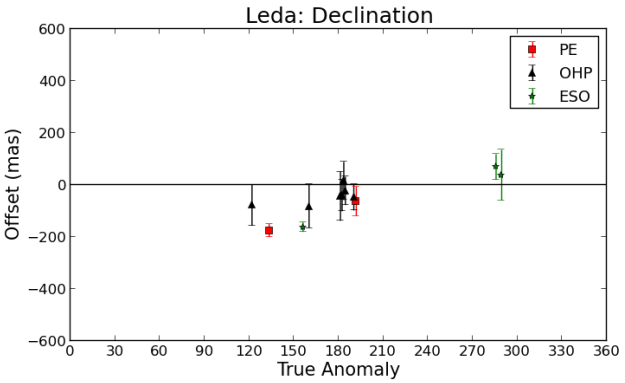

(b) Declination

Fig. A.4. Same as in Fig A.1 for Leda.

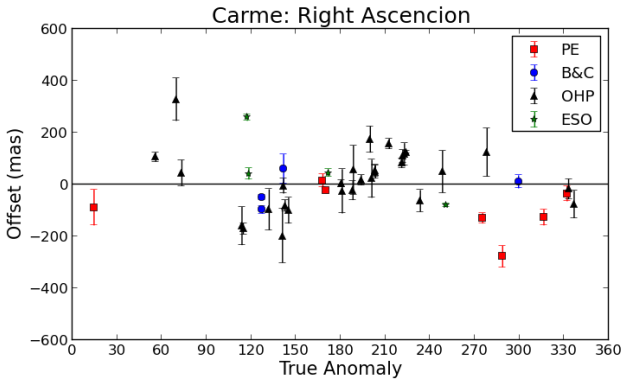

(a) Right Ascension

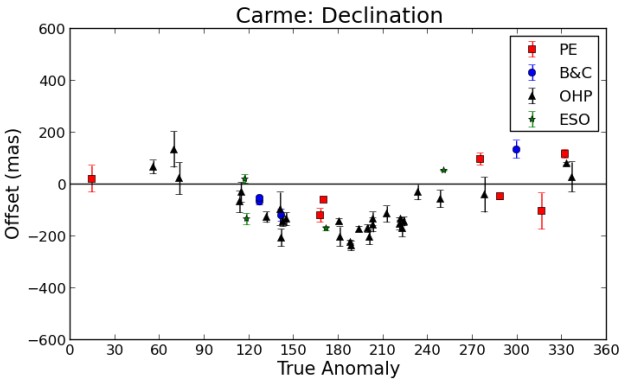

(b) Declination

Fig. A.5. Same as in Fig A.1 for Carme.

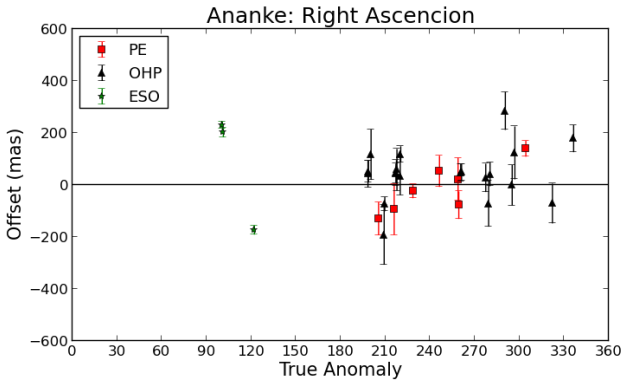

(a) Right Ascension

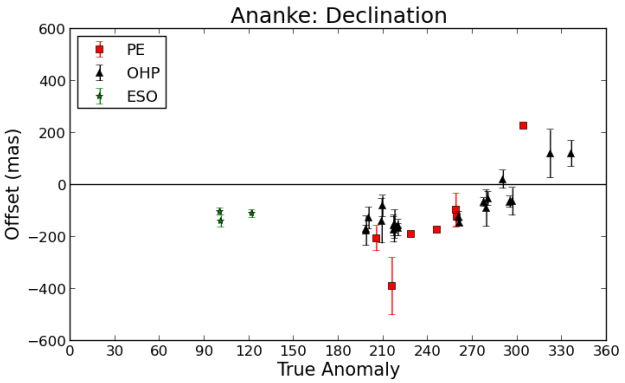

(b) Declination

Fig. A.6. Same as in Fig A.1 for Ananke.

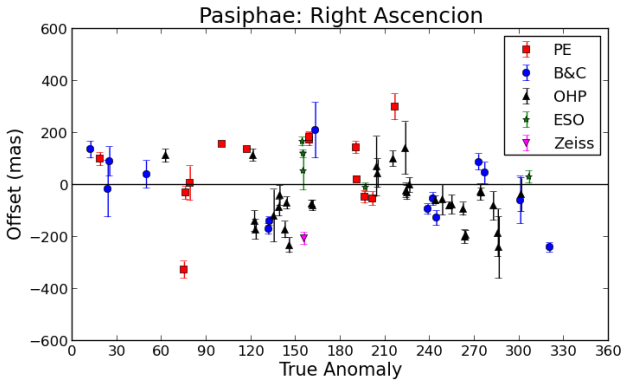

(a) Right Ascension

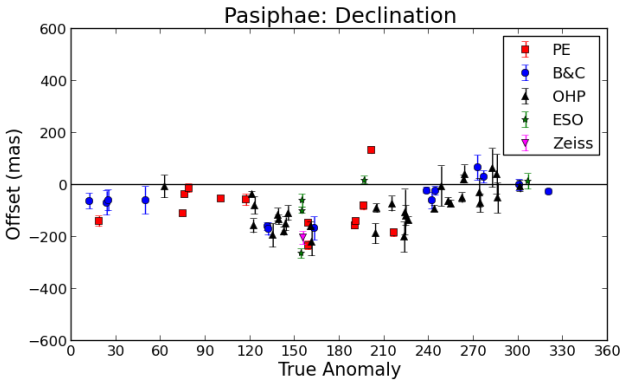

(b) Declination

Fig. A.7. Same as in Fig A.1 for Pasiphae.

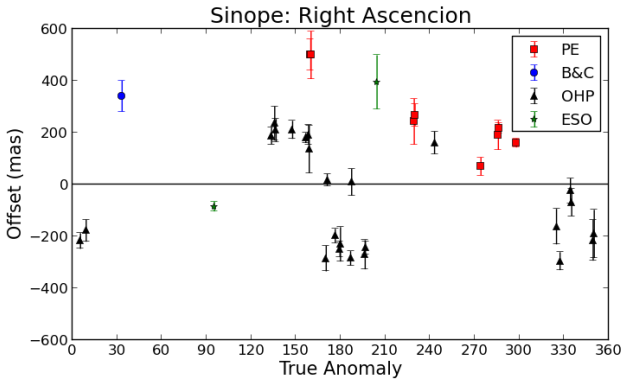

(a) Right Ascension

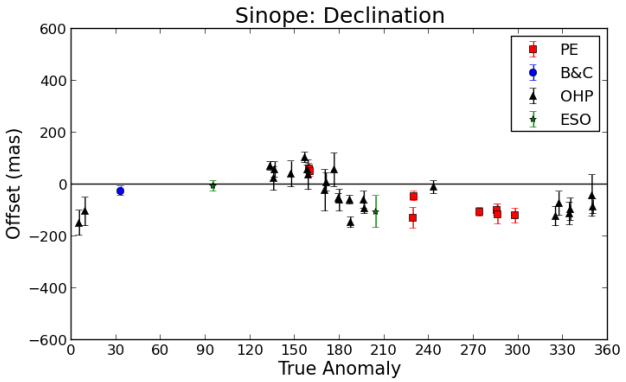

(b) Declination

Fig. A.8. Same as in Fig A.1 for Sinope.

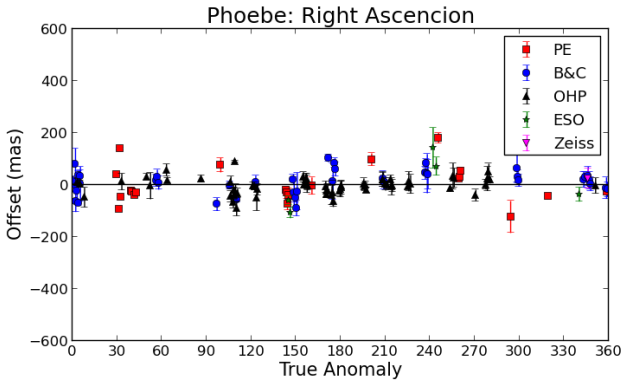

(a) Right Ascension

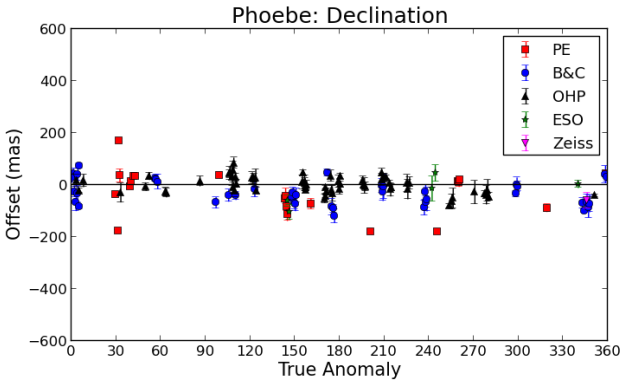

(b) Declination

Fig. A.9. Same as in Fig A.1 for Phoebe.

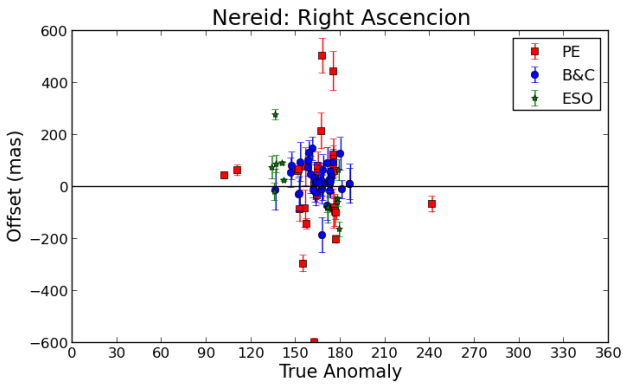

(a) Right Ascension

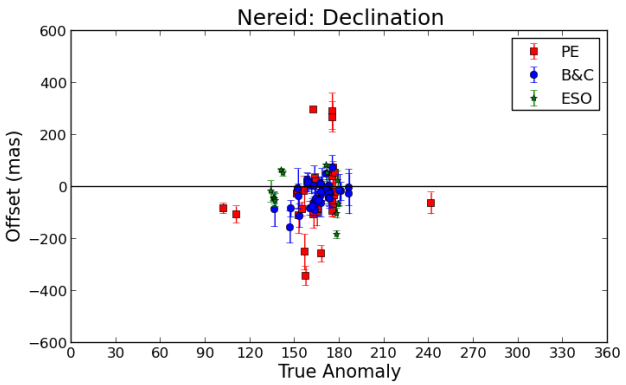

(b) Declination

Fig. A.10. Same as in Fig A.1 for Nereid.